

# Impact of nuclear vibrations on van der Waals and Casimir interactions at zero and finite temperature

Prashanth S. Venkataram,<sup>1</sup> Jan Hermann,<sup>2</sup> Teerit J. Vongkavit,<sup>3</sup> Alexandre Tkatchenko,<sup>2</sup> and Alejandro W. Rodriguez<sup>1</sup>

<sup>1</sup>*Department of Electrical Engineering, Princeton University, Princeton, New Jersey 08544, USA*

<sup>2</sup>*Physics and Materials Science Research Unit, University of Luxembourg, L-1511 Luxembourg*

<sup>3</sup>*Department of Physics, Princeton University, Princeton, New Jersey 08544, USA*

(Dated: October 9, 2018)

Van der Waals (vdW) and Casimir interactions depend crucially on material properties and geometry, especially at molecular scales, and temperature can produce noticeable relative shifts in interaction characteristics. Despite this, common treatments of these interactions ignore electromagnetic retardation, atomism, or contributions of collective mechanical vibrations (phonons) to the infrared response, which can interplay with temperature in nontrivial ways. We present a theoretical framework for computing electromagnetic interactions among molecular structures, accounting for their geometry, electronic delocalization, short-range interatomic correlations, dissipation, and phonons at atomic scales, along with long-range electromagnetic interactions among themselves or in the vicinity of continuous macroscopic bodies. We find that in carbon allotropes, particularly fullerenes, carbyne wires, and graphene sheets, phonons can couple strongly with long-range electromagnetic fields, especially at mesoscopic scales (nanometers), to create delocalized phonon polaritons that significantly modify the infrared molecular response. These polaritons especially depend on the molecular dimensionality and dissipation, and in turn affect the vdW interaction free energies of these bodies above a macroscopic gold surface, producing nonmonotonic power laws and nontrivial temperature variations at nanometer separations that are within the reach of current Casimir force experiments.

Van der Waals (vdW) interactions play an integral role in binding and interaction energies of molecules in condensed phases [1–3], and their long-range many-body nature [3–7] can modify phonons in molecular crystals to the extent of producing qualitatively different predictions of thermodynamic stability at finite temperature compared to common pairwise approximations [8–10]. However, while these treatments of many-body vdW interactions account for multiple scattering and electromagnetic (EM) screening to all orders and derive material properties from ab-initio calculations, they only account for valence electrons and not phonons in the molecular response, despite the large role of the latter in interactions at finite temperature; moreover, these treatments neglect electromagnetic retardation, which becomes important at length scales where phononic contributions to molecular response become important too. Such accounts of phonons have more typically arisen in continuum treatments of Casimir interactions, where polarizable objects are modeled as dipoles or continuum local dielectrics with infrared resonances determined empirically [11–13]. In the related domain of thermal radiation, vibrational resonances have been treated atomistically via mechanical Green’s function [14–19] as well as molecular dynamics [20–23] methods, but these have the respective pitfalls of being limited to bulk materials or using heuristic pairwise approximations to noncovalent interactions.

In this paper, we develop and apply a framework for computing retarded, many-body (RMB) vdW interactions in mesoscopic systems, where molecules can be treated in an ab-initio atomistic way and larger bodies can be treated via continuum electrodynamics, to include the impact of phonons and dissipation in molecular response as well as finite temperature, based on related recent developments [24]. In particular, we focus on the interactions of fullerenes, carbyne wires,

and graphene sheets with a gold surface, which we approximate as a perfect electrically conducting plane for computational simplicity, and compare interaction energies with and without phonon contributions at  $T = 0$  and  $T = 300$  K to each other, as well as to predictions from dipolar and continuum treatments where appropriate. We find that phonons can significantly delocalize the molecular response, which is especially relevant when the molecule is close to the surface, in a manner strongly dependent on the molecular dimensionality, size, and dissipation properties, due to the shape-dependent coupling of those phonons with EM fields to form phonon polaritons. Moreover, in contrast to common macroscopic treatments of Casimir forces in bulk media, which find nontrivial temperature effects only at large separations of at least 1 micron [25], we find that phonon-induced nonlocality can lead to temperature-sensitive vdW interactions even at small separations. In particular, we show that “0-dimensional” fullerenes retain a relatively localized response and consequently lesser deviations of finite from zero-temperature free energies and power laws at nanometer separations, while “1-dimensional” carbyne wires exhibit much larger quantitative but also qualitative deviations, including nonmonotonic power laws. By contrast, “2-dimensional” graphene sheets have many more avenues for dissipation and stronger bonds than isolated compact molecules, leading to damping of the nonlocal response, in which case finite temperature effects, while larger than previously predicted, only become evident at larger (tens of nanometers) separations. We expect our predictions to be relevant to ongoing experiments on vdW interactions among molecules and metallic objects at nanometric scales [26].

**Method.**—At temperature  $T$ , the free energy of interaction among a collection of  $N_{\text{mol}}$  disjoint molecules labeled  $l$ , with electric susceptibilities  $\nabla_l$ , and macroscopic bodies with

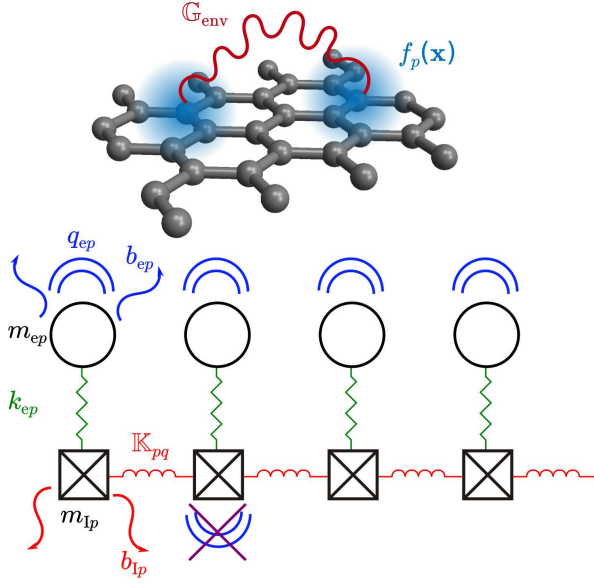


Figure 1. **RMB model of molecular response.** A collection of atoms with electronic polarization response modeled as Gaussian basis functions  $f_p(\mathbf{x})$  interact via long-range electromagnetic fields  $\mathbb{G}_{\text{env}}$ . The individual electronic response of each atom arises from the coupling of valence electronic and phononic excitations via short-range interactions, represented schematically: for every atom  $p$ , a nuclear oscillator of mass  $m_{I_p}$  with dissipation  $b_{I_p}$  is connected to nuclear oscillators of other atoms  $q$  via anisotropic spring constants  $\mathbb{K}_{pq}$ , and to an electronic oscillator of mass  $m_{ep}$  with dissipation  $b_{ep}$  and isotropic spring constant  $k_{ep}$ ; only the electrons couple directly to long-range EM fields with effective charge  $q_{ep}$ .

a composite susceptibility  $\mathbb{V}_{\text{env}}$  is given by [24, 27, 28],

$$\mathcal{F} = k_B T \sum_{n=0}^{\infty} \underbrace{\ln(\det(\mathbb{T}_{\infty} \mathbb{T}^{-1}))}_{\Phi(i\xi_n)}. \quad (1)$$

whose integrand  $\Phi(i\xi)$  depends on the inverse of the scattering “ $\mathbb{T}$ ” operator  $\mathbb{T}^{-1} = \sum_l \mathbb{V}_l^{-1} - \mathbb{G}_{\text{env}}$ , which encodes EM scattering to all orders among the molecules mediated by the continuum bodies, and  $\mathbb{T}_{\infty}^{-1} = \prod_l \mathbb{T}_{l\infty}^{-1}$ , which encodes the scattering properties of each molecule isolated in vacuum,  $\mathbb{T}_{l\infty}^{-1} = \mathbb{V}_l^{-1} - \mathbb{G}_0$ ;  $\mathbb{G}_{\text{env}}$  denotes the imaginary-frequency Green’s function of the macroscopic bodies, which solves the macroscopic Maxwell’s equations (setting  $\epsilon_0 = 1$ ):

$$\left[ \nabla \times \nabla \times + \frac{\xi^2}{c^2} (\mathbb{I} + \mathbb{V}_{\text{env}}) \right] \mathbb{G}_{\text{env}} = \mathbb{I}. \quad (2)$$

Note that all of these quantities depend on frequency, but this is notationally suppressed for brevity. The integrand  $\Phi$  is evaluated at imaginary Matsubara frequencies  $\xi_n = \frac{2\pi k_B T n}{\hbar}$ , with the prime on the summation denoting the  $n = 0$  term contributing a half-weight relative to the other terms and the  $T \rightarrow 0$  limit reducing to an integral over all  $\xi$ .

While the vacuum EM Green’s function  $\overset{\leftrightarrow}{G}_0(i\xi, \mathbf{x}, \mathbf{x}') = (\mathbb{I} - \frac{c^2}{\xi^2} \nabla \otimes \nabla) \frac{e^{-\xi|\mathbf{x}-\mathbf{x}'|/c}}{4\pi|\mathbf{x}-\mathbf{x}'|}$  is known analytically,  $\mathbb{G}_{\text{env}}$  and

$\mathbb{V}_l$  typically must be constructed numerically. The former can be done using one of many available classical EM techniques [1, 12, 29, 30]. The latter in principle requires descriptions accounting for the quantum delocalization and transitions of electrons, and while the susceptibilities  $\mathbb{V}_l$  are basis-independent quantities, computational treatment of electromagnetic interactions between arbitrarily delocalized electrons becomes challenging. However, recent work in the context of vdW interactions [3, 4, 6, 31] has demonstrated accurate results by expressing the molecular susceptibilities,

$$\mathbb{V}_l = -\frac{\xi^2}{c^2} \sum_{p,i,q,j} \alpha_{pi,qj} |\mathbf{f}_{pi}\rangle \langle \mathbf{f}_{qj}|, \quad (3)$$

in terms of localized basis functions  $|\mathbf{f}_{pi}\rangle$  representing the EM response of valence electrons via dipolar ground state wavefunctions of effective polarizabilities  $\alpha$ . We briefly describe the construction of the molecular response functions  $\mathbb{V}_l$  and their underlying assumptions, shown schematically in Fig. 1, and leave more detailed descriptions to Appendix A. For the insulating and weakly metallic molecular systems we consider, the ground state electron density is relatively localized around each atom, so once it is found via DFT, it can be partitioned into atomic fragments that incorporate short-range quantum exchange, correlation, hybridization, and electrostatic effects. These fragments are then mapped onto a set of harmonic oscillators for each atom  $p$  in each molecule, namely a single effective electronic oscillator of charge  $q_{ep}$ , mass  $m_{ep}$ , spring constant  $k_{ep}$  connecting only to the nucleus, and damping coefficient  $b_{ep}$ , representing the valence electron, and a single nuclear oscillator of mass  $m_{I_p}$ , anisotropic spring constants  $\mathbb{K}_{pq}$  connecting to other nuclei, and damping coefficient  $b_{I_p}$ , representing the nucleus screened by inner electrons which give rise to phonons.

Within the RMB framework, only the *valence* electronic oscillators are assumed to couple to long-range EM fields via their charges  $q_{ep}$ , thereby giving rise to the molecular response in the first place, but the features of the response are strongly influenced by the coupling of the electronic oscillators to their corresponding mobile nuclear oscillators via  $k_{ep}$  and the coupling of nuclei to each other via  $\mathbb{K}_{pq}$ ; in particular, the screening of the nuclei by the inner electrons means the tensors  $\mathbb{K}_{pq}$  are typically only nonzero for nearest neighbors [15, 16, 32, 33], and also justifies our assumption that the nuclear oscillators do not couple directly to long-range EM fields. All of these quantities except the damping coefficients  $b_{ep}$  and  $b_{I_p}$  incorporate short-range interaction effects by virtue of being computed from ab-initio DFT calculations or elemental data; in principle, the damping coefficients may also be rigorously derived by coupling these oscillator degrees of freedom to appropriate reservoirs describing the full system, whether the molecule is in vacuum, suspended in a condensed phase, or large enough to support a continuum of phonons that irreversibly carry energy away, but we choose simple approximate values justified by empirical considerations appropriate to each system. These quantities are

collected from all molecules and respectively arranged into  $3N \times 3N$  matrices ( $M_e, Q_e, B_e, K_e, M_I, B_I, K_I$ ) that satisfy the frequency-domain equations of motion [24]

$$\begin{bmatrix} K_e - i\omega B_e - \omega^2 M_e & -K_e \\ -K_e & K_e + K_I - i\omega B_I - \omega^2 M_I \end{bmatrix} \begin{bmatrix} x_e \\ x_I \end{bmatrix} = \begin{bmatrix} Q_e e_e \\ 0 \end{bmatrix} \quad (4)$$

for the electronic and nuclear oscillator displacements ( $x_e, x_I$ ) in terms of the total electric field  $|\mathbf{E}\rangle$  represented in the basis of electronic oscillators as a  $3N$ -dimensional vector  $e_e$ . Solving for the electronic oscillator dipole moment  $p_e = Q_e x_e = \alpha e_e$  yields the electric susceptibility matrix evaluated at frequency  $\omega = i\xi$ ,

$$\alpha = Q_e (K_e + \xi B_e + \xi^2 M_e - K_e (K_e + K_I + \xi B_I + \xi^2 M_I)^{-1} K_e)^{-1} Q_e \quad (5)$$

entering the expansion of  $\mathbb{V}$  above. The nuclear and electronic masses differ by four orders of magnitude, while their respective harmonic coupling strengths are comparable, leading to two frequency scales relevant to the response, with phonons dominating the static and infrared response while valence electrons dominate at visible and ultraviolet imaginary frequencies.

As mentioned above, even though we use DFT to account for the change in electronic polarizability in each atom in a molecule due to its neighbors, our use of oscillators to describe the valence electronic degrees of freedom restricts our consideration to molecular systems that are insulating or weakly metallic; at the level of the bare susceptibility  $\mathbb{V}$ , the valence electronic oscillators by themselves do not display the significant electronic delocalization and mobility inherent in strongly metallic or doped systems, as may be captured in tight-binding and related models. However, short-range internuclear couplings encoded in  $K_I$  give rise to collective nuclear oscillations (phonons) that in turn couple different electronic oscillators to each other; this produces nonlocality (spatial dispersion) in the bare susceptibility  $\mathbb{V}$  in an ab-initio rather than phenomenological way, and in turn ensures that vdW interactions among atoms and molecules remain finite even at vanishing separations, in contrast to point dipolar and continuum treatments [11–13]. In particular, we use Gaussian basis functions [6, 7, 34–38]

$$\mathbf{f}_{pi}(\mathbf{x}) = \left(\sqrt{2\pi}\sigma_p\right)^{-3} \exp\left[-\frac{(\mathbf{x} - \mathbf{r}_p)^2}{2\sigma_p^2}\right] \mathbf{e}_i \quad (6)$$

centered at the equilibrium atomic positions  $\mathbf{r}_p$ , polarized along the Cartesian direction  $\mathbf{e}_i$ , and normalized so that  $|\int \mathbf{f}_{pi}(\mathbf{x}) d^3x| = 1$ . The isotropic widths  $\sigma_p$  of these basis functions have been chosen at each frequency as,

$$\sigma_p(i\xi) = \frac{1}{\sqrt{4\pi}} \left(\frac{|\alpha_p(i\xi)|}{3}\right)^{1/3}, \quad (7)$$

such that a dipolar oscillator of isotropic polarizability  $\alpha_p$  has the same self-interaction energy  $-\frac{\xi^2}{3c^2} \sum_i \langle \mathbf{f}_{pi} | \mathbb{G}_0 | \mathbf{f}_{pi} \rangle$  as that of a Gaussian dipole distribution in vacuum. Without phonons, the bare molecular response  $\mathbb{V}$  would be essentially local, and each valence electronic oscillator would have an individual polarizability  $\alpha_p(i\xi) = q_{ep}^2 / (k_{ep} + \xi b_{ep} + \xi^2 m_{ep})$ , producing widths  $\sigma \sim 1$  angstrom at low frequency. With phonons,  $\mathbb{V}$  is inherently nonlocal, so we extend (7) by defining effective local isotropic atomic polarizabilities

$$\alpha_p(i\xi) = \frac{1}{3} \sum_{q,j} \alpha_{pj,qj}(i\xi) \quad (8)$$

that capture the spatial extent of nonlocal response due to phonons in the atomistic systems we consider, especially at lower frequencies, directly from the properties of the electronic and nuclear oscillators; this atomic contraction effectively constitutes a local approximation to the susceptibility within our oscillator model [39], but used only for constructing the Gaussian widths. The resulting Gaussian widths strongly depend on the molecular geometry, as encoded in nearest-neighbor bonds in the internuclear coupling matrix  $K_I$ . For low-dimensional materials like carbyne or graphene, we observe  $\sigma \sim 1$  nm at low frequencies, with smaller widths arising in compact molecules like fullerenes.

Electromagnetic interactions among electronic oscillators are modified by phonons in two ways, both of which depend strongly on the atomistic geometry and material properties encoded in the oscillator model. The first is that the basis functions  $|\mathbf{f}_{pi}\rangle$  attenuate short-distance EM divergences via the smearing of the valence electronic response. Namely, EM fields can be significantly screened if phonons enhance the magnitude and nonlocality of the electronic response such that  $\sigma$  increases beyond a few bond lengths. The second arises from multiple scattering and screening effects through the mutual coupling of the oscillators via long-range EM fields [4, 6, 7, 39]; this gives rise to effective plasmon-polaritons, as seen through shifts in the oscillator frequencies from the poles of the resulting nonlocal susceptibility,

$$\overleftrightarrow{\chi}(i\xi, \mathbf{x}, \mathbf{x}') = -\frac{c^2}{\xi^2} \langle \mathbf{x} | \mathbb{V} | \mathbf{x}' \rangle = \sum_{p,i,q,j} \alpha_{pi,qj} \mathbf{f}_{pi}(\mathbf{x}) \otimes \mathbf{f}_{qj}(\mathbf{x}'), \quad (9)$$

which includes only short-range interactions, to those of  $\mathbb{T}$ , which include long-range EM interactions as well. This effect is present even in the absence of phonons, in which case the nuclei are taken to be fixed in space as in past work. With phonons, nonlocality may interplay in complex ways with molecular geometry and material properties, producing phonon-polariton resonances that couple nuclear, electronic, and EM degrees of freedom, further modifying the poles of  $\mathbb{T}$ . As we show below, the screening of long-range EM interactions by phonons can modify the behavior of vdW interactions at different distance regimes, especially as a function of temperature. The inherent nonlocality in  $\mathbb{V}$  due to  $K_I$  also implies that in contrast to previous treatments based on local

electronic polarizabilities, the Born approximation of the integrand  $\Phi$  in (1) to low order in EM scattering no longer represents a pairwise summation (PWS) approximation, as the former includes correlations among all atoms due to phonons.

In the following, we study the RMB free energy of interaction at zero and room temperatures between various molecular systems and a planar gold slab, the latter of which we model as a perfect conductor for simplicity in computing  $\mathbb{G}_{\text{env}}$  (via image theory). Specifically, we consider (separately) a  $C_{500}$ -fullerene of radius 1 nm, a long carbyne wire oriented parallel to the surface, and an undoped graphene sheet of infinite extent parallel to the surface; we focus on carbon allotropes because their static electronic polarizabilities are large enough for many-body effects to become particularly evident compared to insulating biological molecules, but their electron densities are localized enough for Hirshfeld partitioning and our oscillator model to remain accurate compared to stronger metals. In each case, we make appropriate comparisons to other predictions which typically make further simplifications beyond our stated assumptions. We compare results both in the presence and absence of phonons, the latter of which is obtained by replacing  $\alpha$  with a purely electronic response  $\alpha_e = Q_e(K_e + \xi B_e + \xi^2 M_e)^{-1} Q_e$ , which modifies the corresponding basis functions,  $\mathbb{T}$ , and  $\mathbb{T}_\infty$ , and leads to a free energy which we denote  $\mathcal{F}_e$ . In addition, we also compare with the Casimir–Polder (CP) approximate free energy  $\mathcal{F}_{\text{CP}}$ , which replaces (1) with,

$$\mathcal{F}_{\text{CP}} = -k_B T \sum_{n=0}^{\infty} \text{Tr} \left[ \hat{\alpha}^{\text{CP}}(i\xi_n) \cdot \hat{\mathbb{G}}_{\text{sca}}(i\xi_n, \mathbf{r}, \mathbf{r}) \right] \quad (10)$$

in terms of  $\mathbb{G}_{\text{sca}} = \mathbb{G}_{\text{env}} - \mathbb{G}_0$ , representing a contraction of the molecule to a dipole at position  $\mathbf{r}$  with an effective polarizability  $\alpha_{ij}^{\text{CP}} = \sum_{p,q} \langle \mathbf{f}_{pi} | \mathbb{T}_{l\infty} \mathbf{f}_{qj} \rangle$  that includes long-range interactions among molecular degrees of freedom in vacuum to infinite order in the scattering, but only to lowest order with the surface. Finally, in the case of graphene, we compare to predictions obtained via common macroscopic (continuum) models [40–45], described in detail in the appendix.

**Fullerene.**—We begin with the case of a “0-dimensional” fullerene above the gold surface [Fig. 2]. An isolated fullerene will not have the same dissipation mechanisms as a fullerene in solution [11], so we neglect the damping coefficients  $B_e$  and  $B_l$ ; however, we constrain the center of mass of this isolated molecule by fixing the positions of two nuclei on opposite sides of the fullerene. At large  $z$ , the finite size of the fullerene is negligible, so it may be treated like a point dipole with respect to scattering from the plate. Without phonons,  $\alpha_e$  is characterized by a single frequency scale arising from the electronic response [Fig. 2(a)], so when the cutoff frequency  $c/z$  falls below that as  $z$  increases [Fig. 2(b)], the power law monotonically approaches the retarded dipolar limit of  $-4$  at  $T = 0$ . At room temperature,  $T = 300$  K, the power law [Fig. 2(c)] will eventually increase to  $-3$  only when  $z$  becomes comparable to the thermal wavelength,  $\hbar c / (k_B T) \approx 7.6 \mu\text{m}$ , because once the cutoff frequency  $c/z$  falls below

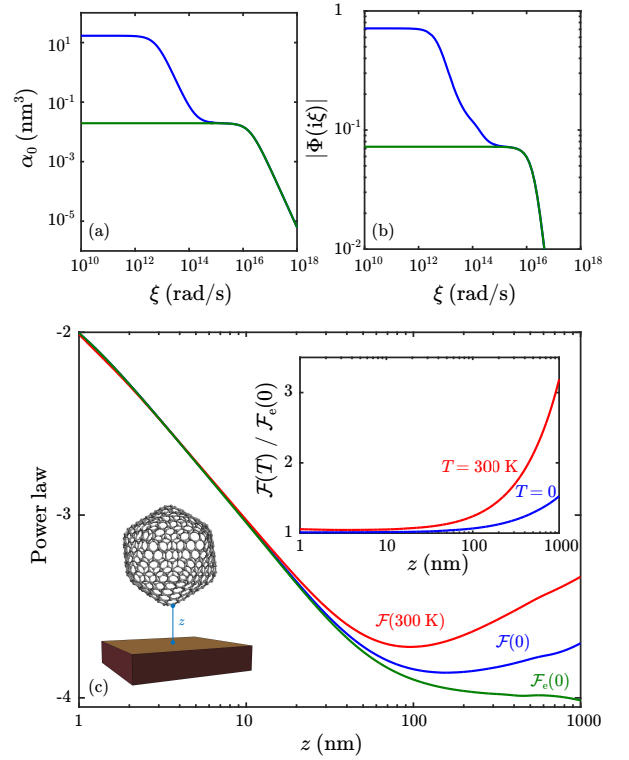


Figure 2. **Impact of phonons at large separations.** (a) Representative polarizability of an individual atomic constituent of a fullerene molecule suspended above a gold plate by a surface–surface gap  $z$ , comparing the full (including phonons)  $\alpha$  (blue) and purely electronic  $\alpha_e$  (green) polarizabilities. (b) RMB free energy integrand  $\Phi(i\xi)$  as a function of imaginary frequency  $\xi$  corresponding to  $\mathcal{F}$  (blue) and  $\mathcal{F}_e$  (green) at a fixed  $z = 1$  nm. (c) RMB power laws for  $\mathcal{F}(0)$  (blue),  $\mathcal{F}(300 \text{ K})$  (red), and  $\mathcal{F}_e(0)$  (green). Inset: energy ratios  $\mathcal{F}(T)/\mathcal{F}_e$  for the fullerene, at  $T = 0$  (blue) or  $T = 300$  K (red).

the first Matsubara frequency  $2\pi k_B T / \hbar$ , only the zero Matsubara frequency will contribute. These predictions are similar to predictions from macroscopic formulations of Casimir physics [11]; namely, in the absence of phonons, the free energies at  $T = 0$  versus  $T = 300$  K are essentially identical for  $z \leq 1 \mu\text{m}$ , like in typical macroscopic situations.

Matters change drastically when phonons are considered, in which case  $\alpha$  is characterized by two frequency scales due to the vastly different nuclear and electronic masses. Even for  $z \leq 1 \mu\text{m}$ , as  $z$  increases, these frequency scales compete with the cutoff frequency  $c/z$  to produce pronounced non-monotonic interaction power laws for  $T = 0$  and  $T = 300$  K; the onset of this deviation based on temperature occurs at separations far smaller than one would expect from common macroscopic predictions, though at large  $z > 7.6 \mu\text{m}$  (which we do not show) the asymptotic power laws approach those observed in the absence of phonons. Such significant sensitivity to temperature at small  $z \approx 100$  nm illustrates that even for a small, compact molecule like fullerene, the interplay between phononic response and long-range EM fields can make

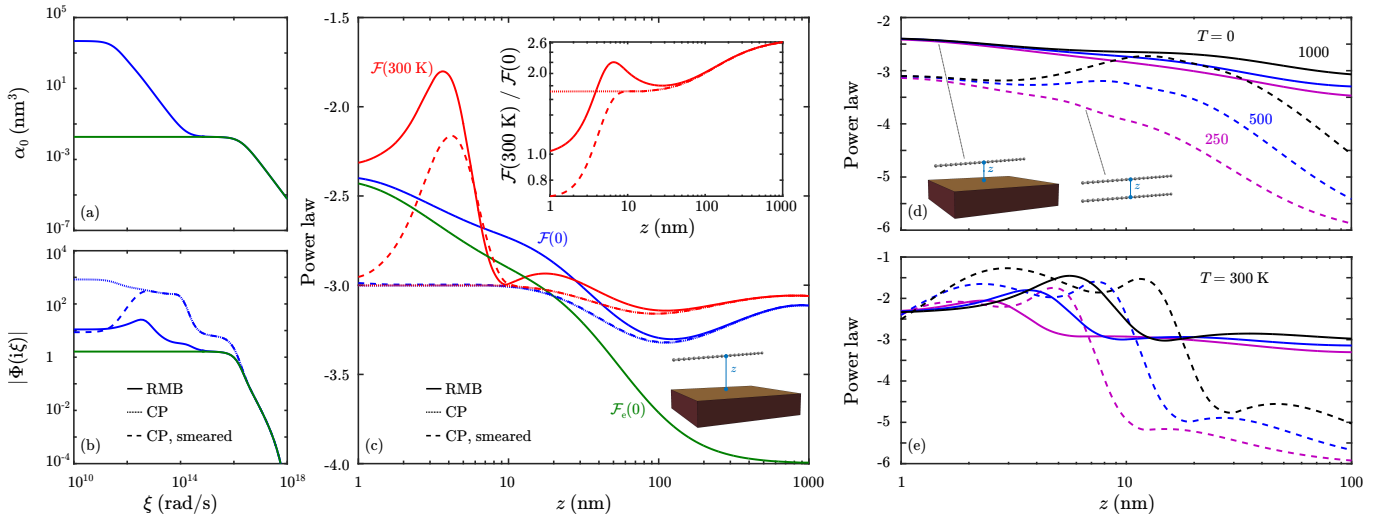


Figure 3. **Nonmonotonicity and temperature deviations due to phonon-induced nonlocal response in an elongated molecule.** (a) Polarizability as a function of imaginary frequency for the middle atom (0) in a 500 atom-long carbyne wire, comparing  $\alpha$  (blue) to  $\alpha_e$  (green). (b) Imaginary frequency integrands for  $\mathcal{F}$  (blue) and  $\mathcal{F}_e$  (green) at  $z = 1$  nm via RMB (solid) or CP, without (fine dashed) or with (coarse dashed) artificial smearing. (c) RMB (solid) and CP, without (fine dashed) or with (coarse dashed) artificial smearing, interaction power laws of a 500 atom-long carbyne wire parallel to a gold plate, for  $\mathcal{F}(0)$  (blue),  $\mathcal{F}(300\text{ K})$  (red), and  $\mathcal{F}_e(0)$  (green). Inset: Free energy ratios  $\mathcal{F}(300\text{ K})/\mathcal{F}(0)$  as functions of  $z$  via RMB (solid) or CP, without (fine dashed) or with (coarse dashed) artificial smearing. (d, e) Power laws for the vdW interactions of one parallel carbyne wire with a gold plate (solid) or two such wires in vacuum (dashed) for wires made of 250 (magenta), 500 (blue), or 1000 (black) atoms, at  $T = 0$  (d) or  $T = 300\text{ K}$  (e).

the interaction power laws deviate significantly from typical macroscopic predictions. The increased relative importance of phononic response at large  $z$  also leads to strong deviations of the free energy ratios  $\mathcal{F}(T)/\mathcal{F}_e(0)$  from 1 for large  $z$  at both values of  $T$  [Fig. 2(c)]. At smaller separations, the finite size and curved spherical shape of the fullerene dominate the interaction power law. Due to the small size of the fullerene, at larger frequencies  $\sim c/z$ , phonons neither significantly delocalize the molecular response nor strongly couple to EM fields, consistent with the fact that Gaussian widths throughout the molecule are smaller than the smallest value of  $z = 1$  nm considered here. Hence, all three power laws converge upon each other for  $z \in [1\text{ nm}, 10\text{ nm}]$ , and the free energy ratios converge to 1 in this limit too. It is worth noting that at  $z \approx 100$  nm, where the power laws exhibit nonmonotonic behavior, the vertical vdW force on the fullerene by the surface is on the order of  $10^{-18}$  N, which is far smaller than currently measurable in state-of-the-art vdW or Casimir force experiments [26, 46–48].

**Carbyne.**—We now turn to the case of a “1-dimensional” carbyne wire [Fig. 3]. As with the fullerene, we assume the damping coefficients  $B_e$  and  $B_l$  to be negligible when the molecule is in isolation, and constrain the nuclei at each end of the wire to remain fixed. While the qualitative behaviors of the interaction power laws  $\partial \ln(\mathcal{F})/\partial \ln(z)$  for a wire at large  $z$  above a gold plate are similar to those of the fullerene, the elongated shape of the wire allows it to support longer-wavelength phonons which couple much more strongly to low-frequency and infrared EM fields, leading to a richer dependence on separation and temperature even for  $z < 100$  nm.

To better understand the physics of these interactions, we compare the RMB predictions to those from the CP approximation of (10), first for a 500 atom-long carbyne wire above a gold plate, and then for various configurations of wire lengths (both in vacuum and above a plate).

For a 500 atom-long carbyne wire, delocalization in the response due to phonons has the strongest effect at low frequencies, leading to static Gaussian basis function widths  $\sigma_0(\omega \rightarrow 0) \approx 3.3$  nm at the middle of the wire. Figure 3(a) plots  $\alpha_0 \sim \sigma_0(i\xi)^3$  as a function of  $\xi$ , showing the existence of two characteristic frequency scales arising from the much stronger phonon-induced electronic delocalization at infrared wavelengths. In contrast, the response in the absence of phonons exhibits only a single frequency scale and the Gaussian widths never exceed 1 angstrom. These enlarged Gaussian smearing widths lead to nonmonotonicity in the RMB integrand [Fig. 3(b)] with respect to  $\xi$  for  $z < \sigma_0(0)$ , as the Gaussian basis functions overlap with the response of the gold plate (i.e. interactions with image basis functions in the perfectly conducting limit). Such non-monotonicity cannot be observed in the absence of phonons, as the bare susceptibility  $\tilde{\chi}(i\xi, \mathbf{x})$  is essentially local in that case. However, as this nonmonotonicity occurs for very small  $\xi$  in the integrand, the behavior of the RMB power law at  $T = 0$  with phonons with respect to  $z$  is less sensitive to the nonmonotonic integrand, simply approaching the power law without phonons as  $z$  decreases [Fig. 3(c)]. By contrast, at  $T = 300\text{ K}$ , the RMB power law with phonons shows significant deviations from that at  $T = 0$  even up to  $z < 20$  nm; essentially, the sampling of Matsubara frequencies at room temperature makes the free

energy disproportionately sensitive to the response at static and infrared  $\xi$ . Additionally, the sensitivity of these vdW interactions at room temperature to the response at infrared and smaller  $\xi$  leads to a free energy ratio  $\mathcal{F}(T)/\mathcal{F}(0)$  that exceeds 2 even for  $z < 20$  nm, and that energy ratio is nonmonotonic because the zero and room temperature RMB free energy power laws with phonons cross each other. At large  $z$ , the magnitude of the RMB free energy ratio  $\mathcal{F}(300 \text{ K})/\mathcal{F}(0)$  is consistent with recent work by Maghrebi *et al.* [49], which shows the sensitivity of this energy ratio to geometry for continuum objects even in the absence of nonlocal response. Note that at  $z = 4$  nm, the vertical force on the wire at  $T = 0$  is  $F_z \approx 10^{-11}$  N, and as can be observed from the power laws and energy ratios, the force ratio is  $\frac{F_z(300 \text{ K})}{F_z(0)} \approx 1.2$ ; both the forces themselves and their differences with respect to temperature should therefore be measurable and resolvable in state-of-the-art Casimir experiments [50], though it should be pointed out that that long free-standing carbyne wires have not been stably fabricable, and carbyne has only been found in solution or confined to supramolecular structures like carbon nanotubes [51, 52].

To better understand these phenomena, we compare these results to those obtained by the CP approximation, where the phonon polaritonic response is contracted into a point dipolar polarizability. In the CP approximation, the integrand is always monotonic, and the power laws at each temperature are monotonic for  $z < 20$  nm, approaching the nonretarded dipolar limit of  $-3$  as  $z$  decreases. This is because in the point dipolar limit, even if the magnitude of the polarizability is enhanced due to phonon polaritons, there is no sense in which nonlocality is captured in its long-range EM interactions. The monotonic decrease in the CP integrand over a very small frequency range also means that even at small  $z$ , Matsubara summation at  $T = 300$  K leads to a significantly larger energy due to contributions from small  $\xi$  than continuous integration over  $\xi$  at  $T = 0$ , so the energy ratio is significantly larger than 1. However, if one artificially smears this point dipole into an isotropic Gaussian distribution of width  $\sigma_0(i\xi)$ , such that the dipole at small  $\xi$  will overlap with its image in the conducting plane for  $z < \sigma_0(0)$ , one qualitatively recovers the nonmonotonic integrand and room temperature power laws. Notably, however, such a “smeared CP approximation” still leads to quantitative differences compared to RMB, as it neglects explicit consideration of the finite molecular size and geometry. For  $z > \sigma_0(0)$ , the smeared CP approximation produces power laws identical to those of the standard CP approximation, and both converge to the corresponding RMB power laws at each respective temperature at much larger  $z$ .

Strictly speaking, for a wire parallel to a conducting plane, modeling the latter via a local macroscopic susceptibility becomes questionable for  $z < \sigma_0(0)$ , as we expect the atomism and spatially dispersive response of the latter to matter more for such small separations. Such an issue is not relevant when considering interactions between two molecules in vacuum. We further explore this by comparing the RMB interaction power laws (in the presence of phonons) of a single car-

byne wire above the gold plate, equivalent to a wire interacting with its correlated image, against that of two parallel, uncorrelated wires interacting in vacuum. In particular, we study wires comprising of either 250, 500, or 1000 atoms at zero [Fig. 3(d)] and room [Fig. 3(e)] temperatures. At  $T = 0$ , the power laws for a single wire above the plate are all monotonic even at small  $z$ , because the free energy is not sensitive to the nonmonotonic integrand for  $z < \sigma_0(0)$ ; essentially, the wire is interacting with its correlated image, which dramatically changes the phonon polaritons emerging from the long-range EM interactions, compared to those of the wire in vacuum. In contrast, the power laws for two wires of at least 500 atoms in vacuum show nonmonotonicity for  $z > 10$  nm, which is larger than  $\sigma_0(0)$  and hence cannot be attributed to overlapping Gaussian basis functions. At  $T = 300$  K, the power laws for a single wire above the plate show nonmonotonicity only for  $z \lesssim \sigma_0(0)$  for every wire length, while the power laws for two wires in vacuum show two maxima for  $z < 20$  nm, with the one at larger  $z$  corresponding to the aforementioned maxima visible for two wires even at  $T = 0$  and occurring in the absence of overlapping Gaussian widths. Thus, it is clear that as nonmonotonic vdW interaction power laws can be observed at room temperature for separations both on the order or larger than the corresponding Gaussian smearing widths, and is therefore not an artifact of overlapping response functions or the lack of atomism in our description of the plate.

**Graphene.**—Finally, we consider a “2-dimensional” infinite graphene sheet above the gold plate. Unlike fullerene molecules or carbyne wires, atomically thin graphene sheets can be exfoliated and suspended in vacuum [53, 54]; therefore, compared to the other aforementioned carbon allotropes, there is significantly more theoretical and experimental work characterizing the mechanical and vibrational [55–57], electronic [58], and thermal [59] properties of graphene. In the particular context of vdW interactions, several theoretical macroscopic models for the response of graphene have been employed, which we summarily describe in the appendix. In what follows, we compare our predictions to those obtained from a Lifshitz formula of the Casimir interaction between a graphene and a plate, based on a tight-binding model of the electronic band structure of graphene. Such a model is consistent with the random phase approximation (RPA) [45] and includes spatial dispersion and the possibility of doping, but does not consider contributions from phonons or dissipation.

As with fullerene and carbyne, the RMB model of the response of graphene partitions the quantum ground-state density into atomic fragments, which are then mapped to a set of effective valence electronic and nuclear oscillators. While the ground-state density encodes similar physics contained in tight-binding Hamiltonians [40–42], the RMB framework require consideration of long-range EM interactions to observe the emergence of electron delocalization (plasmon polaritons). Moreover, the use of localized electron densities in the oscillator model restricts us to consideration of undoped graphene sheets, in contrast to the RPA model [45]. Meanwhile, our explicit consideration of phonons as well as dissi-



cussion of the RPA model has thus far neglected doping, if doping is considered even to an arbitrarily small degree, the presence of free mobile charge carriers (plasmons) does lead to a divergence in the RPA susceptibility as  $\mathbf{k} \rightarrow 0$ , providing slightly better qualitative agreement with RMB predictions.

We now compare the predictions of both RMB and RPA models for the vdW interaction free energy per unit area of graphene above a gold plate, at both zero and room temperatures. In particular, Fig. 4(c) shows the free energy power law and corresponding energy ratios, with respect to the gap separation  $z$ . The RPA model is analyzed in the presence and absence of doping, with doping concentration  $n = 10^{13} \text{ cm}^{-2}$ . Our RMB predictions for the power laws are qualitatively similar to those of the fullerene in that the delocalization in the response due to phonons leads to power laws at both temperatures that are nonmonotonic, though the higher dimensionality of graphene compared to fullerene or carbyne causes the onset of nonmonotonic behavior to arise at smaller  $z \gtrsim 20 \text{ nm}$  than for the fullerene or carbyne; while issues of convergence and numerical error limit our consideration to  $z \leq 100 \text{ nm}$ , we expect the RMB power laws to asymptotically approach -3 and -2 at zero and finite temperature, respectively. Likewise, as the impact of phonons is more pronounced at larger temperatures, the energy ratio starts to deviate noticeably from 1 at  $z \gtrsim 20 \text{ nm}$ . Note that at  $z = 100 \text{ nm}$ , the vertical force ratio  $F_z(300 \text{ K})/F_z(0) \approx 1.3$  and corresponding pressure  $F_z/A \approx 1 \text{ N/m}^2$ , and thus these differences should be measurable in state-of-the-art experiments [62, 63]. Compared to our previous predictions in carbyne systems, the assumption of much larger nuclear dissipation  $B_1$  in graphene significantly dampens and smears the impact of long-wavelength acoustic phonons, limiting the phonon mean free path and hence the spatial extent of delocalization in our Gaussian widths  $\sigma$  to a much greater degree. Consequently, we observe energy ratios much closer to 1 and monotonic power laws at small separations  $z \lesssim 20 \text{ nm}$ . Notably, the RPA power law without doping is a constant -3 at zero temperature over all  $z$ , increasing monotonically toward -2 at finite temperatures. With doping, both power laws are observed to increase from -3 for  $z > 10 \text{ nm}$ , though as Sernelius [45] makes clear, these begin to approach their asymptotic values at very large  $z \gg 100 \text{ nm}$ . Finally, since RPA does not include phonons, there is no nonmonotonic behavior in the power laws, and the RPA power laws with or without doping are consistently above -3 in the range of separations  $z$  that we consider, unlike the RMB power laws which drop below -3 for  $z \sim 20 \text{ nm}$ .

**Concluding remarks.**—We have demonstrated the strong influence of nonlocal response arising from phonons on the vdW interactions of molecular systems, particularly highlighting the dependence of these effects on molecular shape, size, temperature, and material dissipation. These effects can conspire to produce changes in the vdW interaction energy, relative to treatments that neglect phonons or finite temperature, which should be measurable with state-of-the-art experiments, particularly at nanometric separations where macroscopic treatments of Casimir forces in bulk media [25, 50]

predict insignificant temperature effects. The characteristics of molecular vibrations (phonons) in our calculations were derived from covalent bond properties, so one might expect more delocalization of electronic response along the bonds than perpendicular to them. This implies that further accuracy in modeling could be achieved by using anisotropic Gaussian widths to account for this anisotropy. For example, in carbyne, the ratio of transverse to longitudinal internuclear spring coupling coefficients between nearest neighbors is 0.04, while this difference is approximately 0.35 in graphene, so the strong anisotropy in the nonlocal response should be captured in the Gaussian widths in order to more accurately model the material response at short separations. Finally, a more accurate comparison between the RMB predictions and those of macroscopic models for undoped graphene requires smaller dissipation rates, which is likely to result in more temperature-sensitive energies (potentially leading to non-monotonic behavior at small  $z$  akin to those observed in carbyne wires). However, the computational complexity of simulating large unit cells supporting more strongly delocalized phonons makes such a demonstration challenging. Furthermore, intuitive interpretation of the RPA power laws is hampered by the complicated form of the susceptibility, while comparisons with RMB for doped graphene would require a reformulation of the localized oscillator model to allow for inherently delocalized electronic response along with associated changes to DFT computations, the subject of future work.

*Acknowledgements.*—This work was supported by the National Science Foundation under Grants No. DMR-1454836, DMR 1420541, DGE 1148900, and the Cornell Center for Materials Research MRSEC (award no. DMR-1719875), as well as the Luxembourg National Research within the FNR-CORE program (No. FNR-11360857). PSV thanks Chinmay Khandekar, Weiliang Jin, and Sean Molesky for helpful discussions.

## Appendix A: Model of molecular response

The ground-state (i.e. zero-temperature) electron density and geometric configuration of nuclei are determined for each molecule  $l$  separately in isolation by minimizing the energy of the molecule computed via density functional theory (DFT) in the Born–Oppenheimer approximation: for each set of fixed nuclear coordinates, the ground-state electron density is obtained via DFT, and through this, the nuclear coordinates are varied to reach an overall minimum energy, so this process produces ground-state densities and nuclear coordinates that account for short-range quantum exchange, correlation, hybridization, and electrostatic effects. In the insulating or weakly metallic molecular systems that we consider, the electronic wavefunctions are somewhat localized, allowing for a Hirshfeld partitioning of the ground state electron density over the molecule into atomic fragments that account for the presence of other nearby atoms; these atomic fragments are then used with the electron densities of the corresponding isolated



atoms to produce static electronic polarizabilities  $\alpha_{ep}(0)$  associated with each atom  $p$ .

As illustrated schematically in Fig. 1, for each molecule  $l$ , we map onto the set of  $N_l$  atoms labeled by  $p$  (denoting the total number of atoms by  $N = \sum_l N_l$ ) a set of coupled harmonic oscillator degrees of freedom. In particular, each atom  $p$  consists of a single nuclear oscillator, representing the nucleus screened by the inner electrons, and a single electronic oscillator representing the effective valence electrons; this effectively represents an Unsöld approximation [39], which in principle could be relaxed by assigning multiple oscillators to account for many different possible electronic transitions. Within the Unsöld approximation, for the purpose of constructing the molecular response, the electronic oscillator in each atom is initially taken to be undamped (with dissipation to be added later); given  $\alpha_{ep}(0)$ , the electronic oscillator frequencies  $\omega_{ep}$  are computed by fitting the oscillator dispersion to nonretarded vdW  $C_6$ -coefficients for each atom taken from a large reference of theoretical and experimental atomic and small molecular data [4, 6, 39]. From this, the effective number of electrons  $n_{ep}$  associated with that atom can be determined, and so can the effective charge  $q_{ep} = n_{ep}q_e$ , mass  $m_{ep} = n_{ep}m_e$ , and isotropic spring constant  $k_{ep}$ ; these quantities, by virtue of deriving from  $\alpha_{ep}(0)$  and  $\omega_{ep}$ , encode the same short-range quantum and electrostatic effects present in DFT and other high-level quantum calculations [6, 7, 34–38]. The nuclear masses are taken from elemental data as they are four orders of magnitude larger than the electronic masses, while the internuclear spring constants  $\mathbb{K}_{pq}$  are computed as the second spatial derivatives of the ground-state energy in DFT with respect to the nuclear coordinates at equilibrium.

## Appendix B: Model of macroscopic graphene response

Macroscopic treatments of vdW or Casimir interactions involving graphene rely on continuum models of its optical susceptibility, which enter into the familiar Lifshitz formula as idealized reflection coefficients of perfectly thin sheets [1]. These models typically start with quantum-mechanical tight-binding Hamiltonian for the localized  $\pi$ -bonding orbitals [40–45], while neglecting contributions from phonons to the material response and dissipation (though such contributions can be mitigated quantum mechanically through the addition of appropriate coupling [64] and reservoir [60] potentials.) This quantum-mechanical tight-binding electronic Hamiltonian is also commonly approximated as having linear dispersion around the Dirac points, in which case the susceptibility is derived as the lowest-order linear response to an applied perturbative electric field, consistent with the random-phase approximation (RPA). While such a framework is typically presented at zero temperature for analytical convenience, the addition of a Fermi-Dirac distribution in the formula for the linear response allows for consideration of finite temperature effects as well as doping (by varying the chemical potential) on the bare response. Alternative treatments start with

the second-quantized Dirac Hamiltonian of graphene electrons and fields near the Dirac points, ultimately recovering similar expressions for the response in the presence or absence of doping [65–67]. The resulting expressions for the linear EM response explicitly show spatial dispersion. However, only models of doped graphene (which are independent of p- versus n-type doping for the same doping concentration) seem to explicitly consider dissipation, as changing the doping concentration allows for more dissipative mechanisms (e.g. electron-electron or electron-phonon scattering), especially when the chemical potential is far from the Dirac point or when finite temperature is directly used in the construction of the bare response. In the context of vdW interactions, it is also common to simplify these expressions by taking the limit of vanishing parallel wavevector, thereby neglecting spatial dispersion and resulting in relatively small nonlocal length scales in the frequency ranges of interest. Consequently, the response functions follow a similar form as that of Drude or plasma susceptibilities, and in the particular case of undoped graphene, it is common to further approximate the conductivity as having the universal constant  $q_e^2/(16\pi\hbar\epsilon_0)$  over a large range of frequency scales [61, 68, 69]. vdW and Casimir interactions involve integrals over all frequencies (1), in which case the infrared response (including both temporal and spatial dispersion) is expected to be relevant.

To better understand vdW interactions between a graphene sheet and a gold surface, we compare the susceptibility of graphene in our RMB model to an appropriate macroscopic counterpart in the main text. In particular, we use the RPA-derived response of Sernelius [45] (referred to in the main text simply as RPA), with wavevector-dependent permittivity  $\epsilon(\omega, \mathbf{k}) = 1 + \chi(\omega, \mathbf{k})$  defined in terms of the susceptibility

$$\chi(\omega, \mathbf{k}) = \frac{q_e^2 g |\mathbf{k}|}{32\hbar\epsilon_0 \sqrt{v_F^2 |\mathbf{k}|^2 - \omega^2}} \quad (\text{B1})$$

in the undoped case, or

$$\begin{aligned} \chi(\omega, \mathbf{k}) &= \frac{q_e^2 D_0}{2\epsilon_0 |\mathbf{k}|} \left( 1 + \frac{\kappa^2}{4\sqrt{\kappa^2 - \zeta^2}} (\pi - \phi(\kappa, \zeta)) \right) \\ \phi(\kappa, \zeta) &= \arcsin((1 - \zeta)/\kappa) + \arcsin((1 + \zeta)/\kappa) \\ &\quad - \frac{\zeta - 1}{\kappa} \sqrt{1 - \left(\frac{\zeta - 1}{\kappa}\right)^2} + \frac{\zeta + 1}{\kappa} \sqrt{1 - \left(\frac{\zeta + 1}{\kappa}\right)^2} \end{aligned} \quad (\text{B2})$$

in the doped case, for  $\mathbf{k}$  in the plane. These are defined in terms of the Fermi velocity  $v_F = 8.73723 \times 10^5$  m/s and the spin-pseudospin degeneracy  $g = 4$ , as well as the Fermi wavevector  $k_F = \sqrt{4\pi|n|/g}$ , Fermi energy  $E_F = \hbar v_F k_F$ , electron density of states  $D_0 = \frac{\sqrt{g|n|/\pi}}{\hbar v_F}$  at the Fermi level, and dimensionless variables  $\kappa = |\mathbf{k}|/(2k_F)$  and  $\zeta = \hbar\omega/(2E_F)$ . We use these expressions as they capture temporal and spatial dispersion in graphene, while being simpler to manipulate than equivalent expressions derived from second quantization [66, 67]. These expressions for the undoped and

doped macroscopic response may be used for direct comparison with the RMB susceptibility as well as for computing vdW interactions as compared with corresponding RMB predictions; for the latter, as mentioned above, the RPA susceptibilities are used to construct reflection coefficients, which are in turn used in the Lifshitz formula for the Casimir interaction between parallel planar surfaces.

- 
- [1] L. M. Woods, D. A. R. Dalvit, A. Tkatchenko, P. Rodriguez-Lopez, A. W. Rodriguez, and R. Podgornik, "Materials perspective on casimir and van der waals interactions," *Rev. Mod. Phys.* **88**, 045003 (2016).
- [2] D. Langbein, "Theory of van der waals attraction," in *Springer Tracts in Modern Physics* (Springer Berlin Heidelberg, Berlin, Heidelberg, 1974) pp. 1–139.
- [3] A. Tkatchenko, "Current understanding of van der waals effects in realistic materials," *Advanced Functional Materials* **25**, 2054–2061 (2015).
- [4] A. Tkatchenko, A. Ambrosetti, and R. A. DiStasio Jr., "Interatomic methods for the dispersion energy derived from the adiabatic connection fluctuation-dissipation theorem," *The Journal of Chemical Physics* **138**, 074106 (2013).
- [5] V. V. Gobre and A. Tkatchenko, "Scaling laws for van der waals interactions in nanostructured materials," *Nature Communications* **4** (2013), <http://dx.doi.org/10.1038/ncomms3341>.
- [6] R. A. DiStasio Jr., V. V. Gobre, and A. Tkatchenko, "Many-body van der waals interactions in molecules and condensed matter," *Journal of Physics: Condensed Matter* **26**, 213202 (2014).
- [7] A. Ambrosetti, N. Ferri, R. A. DiStasio, Jr., and A. Tkatchenko, "Wavelike charge density fluctuations and van der waals interactions at the nanoscale," *Science* **351**, 1171–1176 (2016).
- [8] A. M. Reilly and A. Tkatchenko, "Role of dispersion interactions in the polymorphism and entropic stabilization of the aspirin crystal," *Phys. Rev. Lett.* **113**, 055701 (2014).
- [9] A. M. Reilly and A. Tkatchenko, "van der waals dispersion interactions in molecular materials: beyond pairwise additivity," *Chem. Sci.* **6**, 3289–3301 (2015).
- [10] J. Hoja, A. M. Reilly, and A. Tkatchenko, "First-principles modeling of molecular crystals: structures and stabilities, temperature and pressure," *Wiley Interdisciplinary Reviews: Computational Molecular Science* **7**, e1294 (2011).
- [11] S. Y. Buhmann, S. Scheel, S. A. Ellingsen, K. Hornberger, and A. Jacob, "Casimir-polder interaction of fullerene molecules with surfaces," *Phys. Rev. A* **85**, 042513 (2012).
- [12] A. W. Rodriguez, F. Capasso, and S. G. Johnson, "The casimir effect in microstructured geometries," *Nature Photonics* **5**, 211–221 (2011).
- [13] J. Zou, Z. Marcet, A. W. Rodriguez, M. T. H. Reid, A. P. McCauley, I. I. Kravchenko, T. Lu, Y. Bao, S. G. Johnson, and H. B. Chan, "Casimir forces on a silicon micromechanical chip," *Nature communications* **4**, 1845 (2013).
- [14] A. Dhar and D. Roy, "Heat transport in harmonic lattices," *Journal of Statistical Physics* **125**, 801–820 (2006).
- [15] Z. Tian, K. Esfarjani, and G. Chen, "Green's function studies of phonon transport across si/ge superlattices," *Phys. Rev. B* **89**, 235307 (2014).
- [16] Z. Tian, K. Esfarjani, and G. Chen, "Enhancing phonon transmission across a si/ge interface by atomic roughness: First-principles study with the green's function method," *Phys. Rev. B* **86**, 235304 (2012).
- [17] N. Mingo and L. Yang, "Phonon transport in nanowires coated with an amorphous material: An atomistic green's function approach," *Phys. Rev. B* **68**, 245406 (2003).
- [18] V. Chiloyan, J. Garg, K. Esfarjani, and G. Chen, "Transition from near-field thermal radiation to phonon heat conduction at sub-nanometre gaps," *Nature communications* **6**, 6755 (2015).
- [19] J. B. Pendry, K. Sasiithlu, and R. V. Craster, "Phonon-assisted heat transfer between vacuum-separated surfaces," *Phys. Rev. B* **94**, 075414 (2016).
- [20] A. Henry and G. Chen, "High thermal conductivity of single polyethylene chains using molecular dynamics simulations," *Phys. Rev. Lett.* **101**, 235502 (2008).
- [21] K. Esfarjani, G. Chen, and H. T. Stokes, "Heat transport in silicon from first-principles calculations," *Phys. Rev. B* **84**, 085204 (2011).
- [22] E. González Noya, D. Srivastava, L. A. Chernozatonskii, and M. Menon, "Thermal conductivity of carbon nanotube peapods," *Phys. Rev. B* **70**, 115416 (2004).
- [23] L. Cui, Y. Feng, and X. Zhang, "Dependence of thermal conductivity of carbon nanopeapods on filling ratios of fullerene molecules," *The Journal of Physical Chemistry A* **119**, 11226–11232 (2015).
- [24] P. S. Venkataram, J. Hermann, A. Tkatchenko, and A. W. Rodriguez, "Unifying microscopic and continuum treatments of van der waals and casimir interactions," *Phys. Rev. Lett.* **118**, 266802 (2017).
- [25] A. Sushkov, W. Kim, D. Dalvit, and S. Lamoreaux, "Observation of the thermal casimir force," *Nature Physics* **7**, 230 (2011).
- [26] C. Wagner, N. Fournier, V. G. Ruiz, C. Li, K. Müllen, M. Rohlfing, A. Tkatchenko, R. Temirov, and F. S. Tautz, "Non-additivity of molecule-surface van der waals potentials from force measurements," *Nature communications* **5**, 5568 (2014).
- [27] S. J. Rahi, T. Emig, N. Graham, R. L. Jaffe, and M. Kardar, "Scattering theory approach to electrodynamic casimir forces," *Phys. Rev. D* **80**, 085021 (2009).
- [28] M. T. H. Reid, J. White, and S. G. Johnson, "Fluctuating surface currents: An algorithm for efficient prediction of casimir interactions among arbitrary materials in arbitrary geometries," *Phys. Rev. A* **88**, 022514 (2013).
- [29] S. G. Johnson, "Numerical methods for computing casimir interactions," in *Casimir Physics*, edited by D. Dalvit, P. Milonni, D. Roberts, and F. da Rosa (Springer Berlin Heidelberg, Berlin, Heidelberg, 2011) pp. 175–218.
- [30] A. W. Rodriguez, P.-C. Hui, D. P. Woolf, S. G. Johnson, M. Lončar, and F. Capasso, "Classical and fluctuation-induced electromagnetic interactions in micron-scale systems: designer bonding, antibonding, and casimir forces," *Annalen der Physik* **527**, 45–80 (2015).
- [31] A. Ambrosetti, A. M. Reilly, R. A. DiStasio, and A. Tkatchenko, "Long-range correlation energy calculated from coupled atomic response functions," *The Journal of Chemical Physics* **140**, 18A508 (2014).
- [32] X. L. Ruan and M. Kaviani, "Enhanced laser cooling of rare-earth-ion-doped nanocrystalline powders," *Phys. Rev. B* **73**, 155422 (2006).
- [33] V. P. Carey, G. Chen, C. Grigoropoulos, M. Kaviani, and A. Majumdar, "A review of heat transfer physics," *Nanoscale and Microscale Thermophysical Engineering* **12**, 1–60 (2008), <http://www.tandfonline.com/doi/pdf/10.1080/15567260801917520>.
- [34] A. G. Donchev, "Many-body effects of dispersion interaction," *The Journal of Chemical Physics* **125**, 074713 (2006).

- [35] A. D. Phan, L. M. Woods, and T.-L. Phan, “Van der waals interactions between graphitic nanowiggles,” *Journal of Applied Physics* **114** (2013), <http://dx.doi.org/10.1063/1.4816446>.
- [36] Y. V. Shtogun and L. M. Woods, “Many-body van der waals interactions between graphitic nanostructures,” *The Journal of Physical Chemistry Letters* **1**, 1356–1362 (2010).
- [37] H.-Y. Kim, J. O. Sofo, D. Velegol, M. W. Cole, and A. A. Lucas, “Van der waals dispersion forces between dielectric nanoclusters,” *Langmuir* **23**, 1735–1740 (2007).
- [38] M. W. Cole, D. Velegol, H.-Y. Kim, and A. A. Lucas, “Nanoscale van der waals interactions,” *Molecular Simulation* **35**, 849–866 (2009).
- [39] J. Hermann, R. A. DiStasio, and A. Tkatchenko, “First-principles models for van der waals interactions in molecules and materials: Concepts, theory, and applications,” *Chemical Reviews* **117**, 4714–4758 (2017), pMID: 28272886, <https://doi.org/10.1021/acs.chemrev.6b00446>.
- [40] B. Wunsch, T. Stauber, F. Sols, and F. Guinea, “Dynamical polarization of graphene at finite doping,” *New Journal of Physics* **8**, 318 (2006).
- [41] T. Wenger, G. Viola, M. Fogelström, P. Tassin, and J. Kinaret, “Optical signatures of nonlocal plasmons in graphene,” *Phys. Rev. B* **94**, 205419 (2016).
- [42] J. F. Dobson, “Dispersion and induction interactions of graphene with nanostructures,” *Surface Science* **605**, 1621–1632 (2011), graphene Surfaces and Interfaces.
- [43] E. H. Hwang and S. Das Sarma, “Dielectric function, screening, and plasmons in two-dimensional graphene,” *Phys. Rev. B* **75**, 205418 (2007).
- [44] M. B. Lundberg, Y. Gao, R. Asgari, C. Tan, B. Van Duppen, M. Autore, P. Alonso-González, A. Woessner, K. Watanabe, T. Taniguchi, R. Hillenbrand, J. Hone, M. Polini, and F. H. L. Koppens, “Tuning quantum nonlocal effects in graphene plasmonics,” *Science* **357**, 187–191 (2017), <http://science.sciencemag.org/content/357/6347/187.full.pdf>.
- [45] B. E. Sernelius, “Retarded interactions in graphene systems,” *Phys. Rev. B* **85**, 195427 (2012).
- [46] S. Tsoi, P. Dev, A. L. Friedman, R. Stine, J. T. Robinson, T. L. Reinecke, and P. E. Sheehan, “van der waals screening by single-layer graphene and molybdenum disulfide,” *ACS Nano* **8**, 12410–12417 (2014), pMID: 25412420, <https://doi.org/10.1021/nn5050905>.
- [47] L. Tang, M. Wang, C. Ng, M. Nikolic, C. T. Chan, A. W. Rodriguez, and H. B. Chan, “Measurement of non-monotonic casimir forces between silicon nanostructures,” *Nature Photonics* **11**, 97 (2017).
- [48] J. L. Garrett, D. A. T. Somers, and J. N. Munday, “Measurement of the casimir force between two spheres,” *Phys. Rev. Lett.* **120**, 040401 (2018).
- [49] M. F. Maghrebí, S. J. Rahi, T. Emig, N. Graham, R. L. Jaffe, and M. Kardar, “Analytical results on casimir forces for conductors with edges and tips,” *Proceedings of the National Academy of Sciences* **108**, 6867–6871 (2011), <http://www.pnas.org/content/108/17/6867.full.pdf>.
- [50] B. E. Sernelius, “Finite-temperature casimir force between metal plates: full inclusion of spatial dispersion resolves a long-standing controversy,” *Journal of Physics A: Mathematical and General* **39**, 6741 (2006).
- [51] W. A. Chalifoux and R. R. Tykwinski, “Synthesis of polyynes to model the sp-carbon allotrope carbyne,” *Nature chemistry* **2**, 967–971 (2010).
- [52] L. Shi, P. Rohringer, K. Suenaga, Y. Niimi, J. Kotakoski, J. C. Meyer, H. Peterlik, M. Wanko, S. Cahangirov, A. Rubio, *et al.*, “Confined linear carbon chains as a route to bulk carbyne,” *Nature materials* **15**, 634 (2016).
- [53] M. Yi and Z. Shen, “A review on mechanical exfoliation for the scalable production of graphene,” *J. Mater. Chem. A* **3**, 11700–11715 (2015).
- [54] J. S. Bunch, A. M. van der Zande, S. S. Verbridge, I. W. Frank, D. M. Tanenbaum, J. M. Parpia, H. G. Craighead, and P. L. McEuen, “Electromechanical resonators from graphene sheets,” *Science* **315**, 490–493 (2007), <http://science.sciencemag.org/content/315/5811/490.full.pdf>.
- [55] L. A. Falkovsky, “Phonon dispersion in graphene,” *Journal of Experimental and Theoretical Physics* **105**, 397–403 (2007).
- [56] M. Endlich, A. Molina-Sánchez, L. Wirtz, and J. Kröger, “Screening of electron-phonon coupling in graphene on ir(111),” *Phys. Rev. B* **88**, 205403 (2013).
- [57] D. Akinwande, C. J. Brennan, J. S. Bunch, P. Egberts, J. R. Felts, H. Gao, R. Huang, J.-S. Kim, T. Li, Y. Li, K. M. Liechti, N. Lu, H. S. Park, E. J. Reed, P. Wang, B. I. Yakobson, T. Zhang, Y.-W. Zhang, Y. Zhou, and Y. Zhu, “A review on mechanics and mechanical properties of 2d materials—graphene and beyond,” *Extreme Mechanics Letters* **13**, 42–77 (2017).
- [58] A. H. Castro Neto, F. Guinea, N. M. R. Peres, K. S. Novoselov, and A. K. Geim, “The electronic properties of graphene,” *Rev. Mod. Phys.* **81**, 109–162 (2009).
- [59] A. A. Balandin, “Thermal properties of graphene and nanostructured carbon materials,” *Nature materials* **10**, 569 (2011).
- [60] J. Li and J. E. Han, “Nonequilibrium excitations and transport of dirac electrons in electric-field-driven graphene,” *Phys. Rev. B* **97**, 205412 (2018).
- [61] O. Ilic, M. Jablan, J. D. Joannopoulos, I. Celanovic, H. Buljan, and M. Soljačić, “Near-field thermal radiation transfer controlled by plasmons in graphene,” *Phys. Rev. B* **85**, 155422 (2012).
- [62] A. A. Banishev, H. Wen, J. Xu, R. K. Kawakami, G. L. Klimchitskaya, V. M. Mostepanenko, and U. Mohideen, “Measuring the casimir force gradient from graphene on a sio<sub>2</sub> substrate,” *Phys. Rev. B* **87**, 205433 (2013).
- [63] G. L. Klimchitskaya and V. M. Mostepanenko, “Comparison of hydrodynamic model of graphene with recent experiment on measuring the casimir interaction,” *Phys. Rev. B* **91**, 045412 (2015).
- [64] M. Jablan, M. Soljačić, and H. Buljan, “Unconventional plasmon-phonon coupling in graphene,” *Phys. Rev. B* **83**, 161409 (2011).
- [65] Y. Barlas, T. Pereg-Barnea, M. Polini, R. Asgari, and A. H. MacDonald, “Chirality and correlations in graphene,” *Phys. Rev. Lett.* **98**, 236601 (2007).
- [66] M. Bordag, I. V. Fialkovsky, D. M. Gitman, and D. V. Vassilevich, “Casimir interaction between a perfect conductor and graphene described by the dirac model,” *Phys. Rev. B* **80**, 245406 (2009).
- [67] M. Bordag, I. Fialkovskiy, and D. Vassilevich, “Enhanced casimir effect for doped graphene,” *Phys. Rev. B* **93**, 075414 (2016).
- [68] D. Drosdoff and L. M. Woods, “Casimir forces and graphene sheets,” *Phys. Rev. B* **82**, 155459 (2010).
- [69] F. H. L. Koppens, D. E. Chang, and F. J. García de Abajo, “Graphene plasmonics: A platform for strong light-matter interactions,” *Nano Letters* **11**, 3370–3377 (2011), pMID: 21766812, <https://doi.org/10.1021/nl201771h>.